11. Ryan, M. J., Fox, J. H., Wilczynski, W. & Rand, A. S. *Nature* **343,** 66–68 (1990).
12. Alcock, J. *Animal Behavior* 5th edn (Sinauer, Sunderland, 1993).
13. Krebs, J. R. & Davies, N. B. *An Introduction of Behavioral Ecology* 3rd edn (Blackwell, Oxford, 1993).
14. Ryan, M. & Rand, A. S. *Phil. Trans. R. Soc.* B **340,** 187–195 (1993).
15. Rosen, D. E. *Bull. Am. Mus. nat. His.* **162,** 268–375 (1979).
16. Rauchenberger, M., Kallman, K. D. & Morizot, D. C. *Am. Mus. nat. His. Nov.* **2975,** 1–41 (1990).
17. Haas, V. in *Trends in Ichthyology* (eds Schröder, J. H., Bauer, J. & Schartl, M.) 279–288 (Blackwell, London, 1993).
18. Basolo, A. L. *Anim. Behav.* **40,** 332–338 (1990).
19. Rosen, D. E. & Bailey, R. M. *Bull. Am. Mus. nat. Hist.* **126,** 1–176 (1963).
20. Swofford, D. L. *Phylogenetic Analysis Using Parsimony* Version 3.1.1 (Illinois Natural History Survey, Champaign, 1993).
21. Saitou, N. & Nei, M. *Molec. Biol. Evol.* **4,** 406–425 (1987).
22. Meyer, M. K. & Schartl, M. *Senkenbergiana biol.* **60,** 147–151 (1980).
23. Morizot, D. C. & Siciliano, M. J. *Genetics* **102,** 539–556 (1982).
24. Dowling, T. E. & DeMarais, B. D. *Nature* **362,** 444–446 (1993).
25. Ryan, M. J. & Wagner, W. E. Jr *Science* **236,** 595–597 (1987).
26. Partridge, L. & Harvey, P. H. *Nature* **328,** 377 (1987).
27. Gordon, M., Cohen, H. & Nigrelli, R. F. *Am. Nat.* **77,** 569–572 (1943).
28. Dzwillo, M. *Verh. Dt. Zool. Ges.* **1962,** 152–159 (1963).
29. Zander, C. D. & Dzwillo, M. *Z. Wissen. Zool.* **178,** 276–315 (1969).
30. Winquist, S. T. *et al. Science* **253,** 1426 (1991).
31. Fisher, R. A. *The General Theory of Natural Selection* 2nd edn (Dover, New York, 1958).
32. Houde, A. & Endler, J. A. *Science* **248,** 1405–1408 (1990).
33. Bakker, T. C. M. *Nature* **363,** 255–257 (1993).
34. Rosen, D. E. & Kallman, K. D. *Am. Mus. nat. His. Nov.* **2379,** 1–29 (1969).
35. Felsenstein, J. *Evolution* **39,** 783–791 (1985).
36. Kocher, T. D. *et al. Proc. natn. Acad. Sci. U.S.A.* **86,** 6196–6200 (1989).
37. Meyer, A., Kocher, T. D., Basasibwaki, P. & Wilson, A. C. *Nature* **347,** 550–553 (1990).
38. Meyer, A. & Lydeard, C. *Proc. R. Soc. Lond.* B **254,** 153–162 (1993).
39. Robertson, S. M. thesis, Ludwigs Maximillians Univ., München (1989).
40. Higgins, D. G. & Sharp, P. M. *CABIOS* **5,** 151–153 (1989).
41. Maddison, W. P. & Maddison, D. R. *MacClade Ver. 3.0. Analysis of Phylogeny and Character Evolution* (Sinauer, Sunderland, 1992).
42. Kumar, S., Tamura, K. & Nei, M. MEGA *Molecular Evolutionary Genetics Analysis* Vers. 1.0 (Inst. of Mol. Evol. Genetics, Pennsylvania State Univ., 1993).
43. Meyer, M. K. *Cour. Forsch.-Inst. Senckenberg* **94,** 123–130 (1987).

ACKNOWLEDGEMENTS. We thank R. Borowsky, J. Endler, R. McKeand and particularly K. Kallmann for specimens; S. Robertson for *X-src* primer design; C. Davis for technical assistance; and A. Basolo, R. Borowsky, J. Endler, K. Kallmann, C. Lydeard, E. Mayr, E. Prager and M. Ryan for comments on the manuscript. Part of this work was completed while A.M. was an Alfred P. Sloan Postdoctoral Fellow in the laboratory of the late Allan C. Wilson at the University of California at Berkeley. A.M. is supported by the US NSF; M.S. is supported by the DFG, Germany.

The generic viewpoint assumption in a framework for visual perception

William T. Freeman

Mitsubishi Electric Research Laboratories, 201 Broadway, Cambridge, Massachusetts 02139, USA

A VISUAL system makes assumptions in order to interpret visual data. The assumption of 'generic view'[1–4] states that the observer is not in a special position relative to the scene. Researchers commonly use a binary decision of generic or accidental view to disqualify scene interpretations that assume accidental viewpoints[5–10]. Here we show how to use the generic view assumption, and others like it, to quantify the likelihood of a view, adding a new term to the probability of a given image interpretation. The resulting framework better models the visual world and reduces the reliance on other prior assumptions. It may lead to computer vision algorithms of greater power and accuracy, or to better models of human vision. We show applications to the problems of inferring shape, surface reflectance properties, and motion from images.

Consider the image of Fig. 1*a*. Perceptually, there are two possible interpretations: a bump, lit from the left, or a dimple, lit from the right. Yet many shapes and lighting directions (Fig. 1*b*) could explain the image. How should a visual system choose?

We note that the ridges in shapes 2–4 of Fig. 1*b* must line up with the assumed light direction. We can study the 'accidentalness' of this alignment by exploring how the image of the illuminated shape changes as we perturb the azimuthal light direction. Figure 1*c* shows that shape 3 presents images similar to that in Fig. 1*a* only for a small range of assumed light directions. The bump in Fig. 1*d* (shape 5) presents images like that in Fig. 1*a* over a broader range of light directions. If all azimuthal light directions are equally likely, shape 5 has more chances to create the image in Fig. 1*a* than does shape 3.

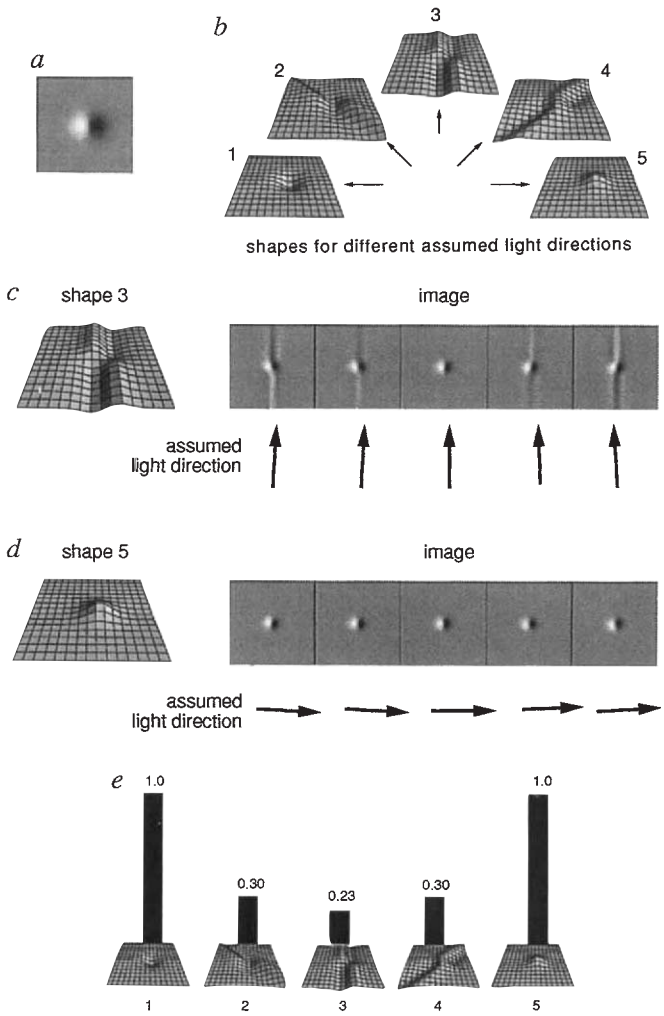

FIG. 1 *a*, Perceptually, this image has two possible interpretations. It could be a bump, lit from the left, or a dimple, lit from the right. *b*, Mathematically, there are many possibilities. The five shown here were found by a linear shape from shading algorithm, assuming shallow incident light from different azimuthal directions and the boundary conditions described in ref. 8. Shapes 2–4 require coincidental alignment with the assumed light direction. For shape 3 in *c*, the rendered image changes quickly with assumed light angle; only a small range of light angles yields an image like that shown in *a*. The generic view term of the scene probability equation, equation (7), penalizes an interpretation that has high image derivatives with respect to the generic variable, in this case light direction. For shape 5 in *d*, a much larger range of light angles gives the observed image. If all light directions are equally likely, shape 5 should be the preferred explanation. The probabilities of the candidate shapes, found using equation (7), are shown in *e*. The results favour shapes 1 and 5, in agreement with the perceptual appearance of *a*.

To quantify such probabilities, we use a bayesian framework (as in ref. 11, for example). This combines the data (Fig. 1*a*) with known or estimated prior probabilities to find the posterior probability of each candidate shape.

We treat the azimuthal light direction as a random variable, an example of what we call a generic variable, $\dot{x}$, with prior probability density $P_{\dot{x}}(\dot{x})$. (We use subscripts to distinguish

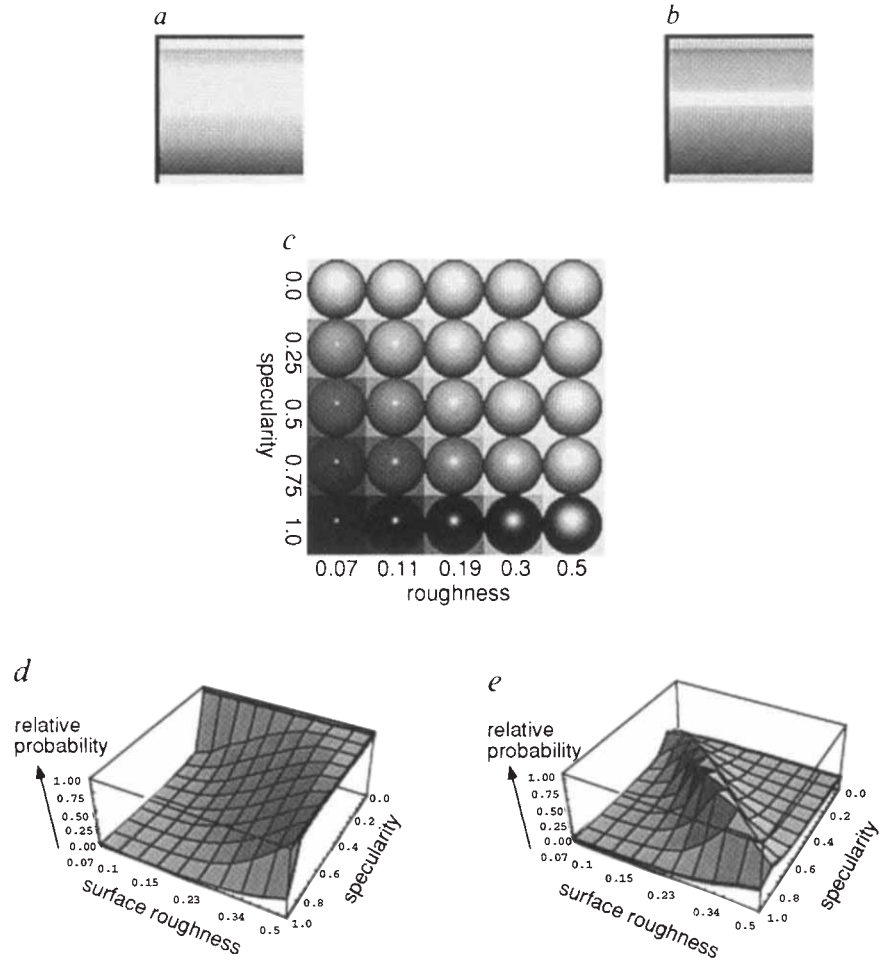

FIG. 2 *a* and *b*, Two images with intensity variations along only one dimension. Such images can be explained by many different combinations of surface reflectance function and shape. We use a two-parameter family of reflectance functions (a subset of the model of ref. 21) and a fixed light position to generate a family of possible shape and reflectance function explanations for each of *a* and *b*. *c*, Visual key to the parameters provided by showing the appearance of the surface reflectance functions, rendered on the surface of a sphere. For every specularity and roughness, shapes exist that produce image *a* or *b*. (For each shape we assumed boundary conditions of constant height at the vertical picture edge.) One wants to choose between these competing explanations without resorting to an *ad hoc* bias toward some shapes or reflectance functions. Each of the explanations will present the images shown over differing ranges of the generic variables, taken here to be vertical light angle and object orientation. The scene probability equation calculates their relative probability densities[22]. Plots *d* and *e* show the probability that the images *a* and *b*, respectively, were created by each surface reflectance function in the parameter space and corresponding shape. The probabilities are the highest for the reflectance functions that look like the material of the corresponding original image (compare with *c*).

between probability densities, P.) Generic variables can include viewpoint, lighting direction, or object pose. These are variables that we do not need to estimate precisely.

We assume a prior probability density, $P_{\vec{\beta}}(\vec{\beta})$, for the scene parameter $\vec{\beta}$ we want to estimate. For this example, shapes 1–5 are assigned equal probabilities. The posterior distribution, $P(\vec{\beta}, \vec{x} \mid \vec{y})$, gives the probability that scene parameter $\vec{\beta}$ (shape) and generic variable $\vec{x}$ (light direction) created the visual data $\vec{y}$ (Fig. 1*a*). From $P(\vec{\beta}, \vec{x} \mid \vec{y})$, we will find the posterior probability $P(\vec{\beta} \mid \vec{y})$.

We use Bayes' theorem to evaluate $P(\vec{\beta}, \vec{x} \mid \vec{y})$:

$$P(\vec{\beta}, \vec{x} \mid \vec{y}) = \frac{P(\vec{y} \mid \vec{\beta}, \vec{x}) P_{\vec{\beta}}(\vec{\beta}) P_{\vec{x}}(\vec{x})}{P_{\vec{y}}(\vec{y})} \tag{1}$$

where we have assumed that $\vec{x}$ and $\vec{\beta}$ are independent. The denominator is constant for all models $\vec{\beta}$ to be compared.

To find $P(\vec{\beta}, \vec{x} \mid \vec{y})$ independently of the value of the generic variable $\vec{x}$, we integrate the joint probability of equation (1) over the possible $\vec{x}$ values:

$$P(\vec{\beta} \mid \vec{y}) = \frac{P_{\vec{\beta}}(\vec{\beta})}{P_{\vec{y}}(\vec{y})} \int P(\vec{y} \mid \vec{\beta}, \vec{x}) P_{\vec{x}}(\vec{x}) \, \mathrm{d}\vec{x} \tag{2}$$

We will assume that the prior probability $P_{\vec{x}}(\vec{x})$ of the generic variables is a constant. The generalization for other priors is straightforward. $P(\vec{y} \mid \vec{\beta}, \vec{x})$ is large where the scene $\vec{\beta}$ and the value $\vec{x}$ give an image similar to the observation $\vec{y}$. The integral of equation (2) integrates the area of $\vec{x}$ for which $\vec{\beta}$ yields the observation. In our example, it effectively counts the frames in Fig. 1*c* or *d*, where the rendered image is similar to the input data.

We assume zero mean gaussian observation noise of variance σ^2, which plays two roles. It measures the similarity between images as the probability that noise accounts for the differences. It can also model physical noise. For this noise model,

$$P(\vec{y} \mid \vec{\beta}, \vec{x}) = \frac{1}{(\sqrt{2\pi\sigma^2})^N} e^{-\|\vec{y} - \vec{f}(\vec{x}, \vec{\beta})\|^2 / 2\sigma^2} \tag{3}$$

where $\vec{f}(\vec{x}, \vec{\beta})$ is a known 'rendering function' which gives the image created by the generic and scene parameters $\vec{x}$ and $\vec{\beta}$, and N is the dimensionality of the visual data $\vec{y}$.

For the low noise limit, we can find an analytic approximation to the integral of equation (2). We expand $\vec{f}(\vec{x}, \vec{\beta})$ in equation (3) in a second-order Taylor series,

$$\vec{f}(\vec{x}, \vec{\beta}) \approx \vec{f}(\vec{x}_0, \vec{\beta}) + \sum_i \vec{f}'_i [\vec{x} - \vec{x}_0]_i + \tfrac{1}{2} \sum_{i,j} [\vec{x} - \vec{x}_0]_i \vec{f}''_{ij} [\vec{x} - \vec{x}_0]_j \tag{4}$$

where $[\,\cdot\,]_i$ indicates the ith component of the vector in brackets, and

$$\vec{f}'_i = \left. \frac{\partial f(\vec{x}, \vec{\beta})}{\partial x_i} \right|_{\vec{x} = \vec{x}_0} \tag{5}$$

and

$$\vec{f}''_{ij} = \left. \frac{\partial^2 \vec{f}(\vec{x}, \vec{\beta})}{\partial x_i \, \partial x_j} \right|_{\vec{x} = \vec{x}_0} \tag{6}$$

We take $\vec{x}_0$ to be the value of $\vec{x}$ which can best account for the observed image data; that is, for which $\|\vec{y} - \vec{f}(\vec{x}, \vec{\beta})\|^2$ is minimized.

Using equations (3)–(6) to second order in $\vec{x} - \vec{x}_0$ in the integral of equation (2), we find the posterior probability for the

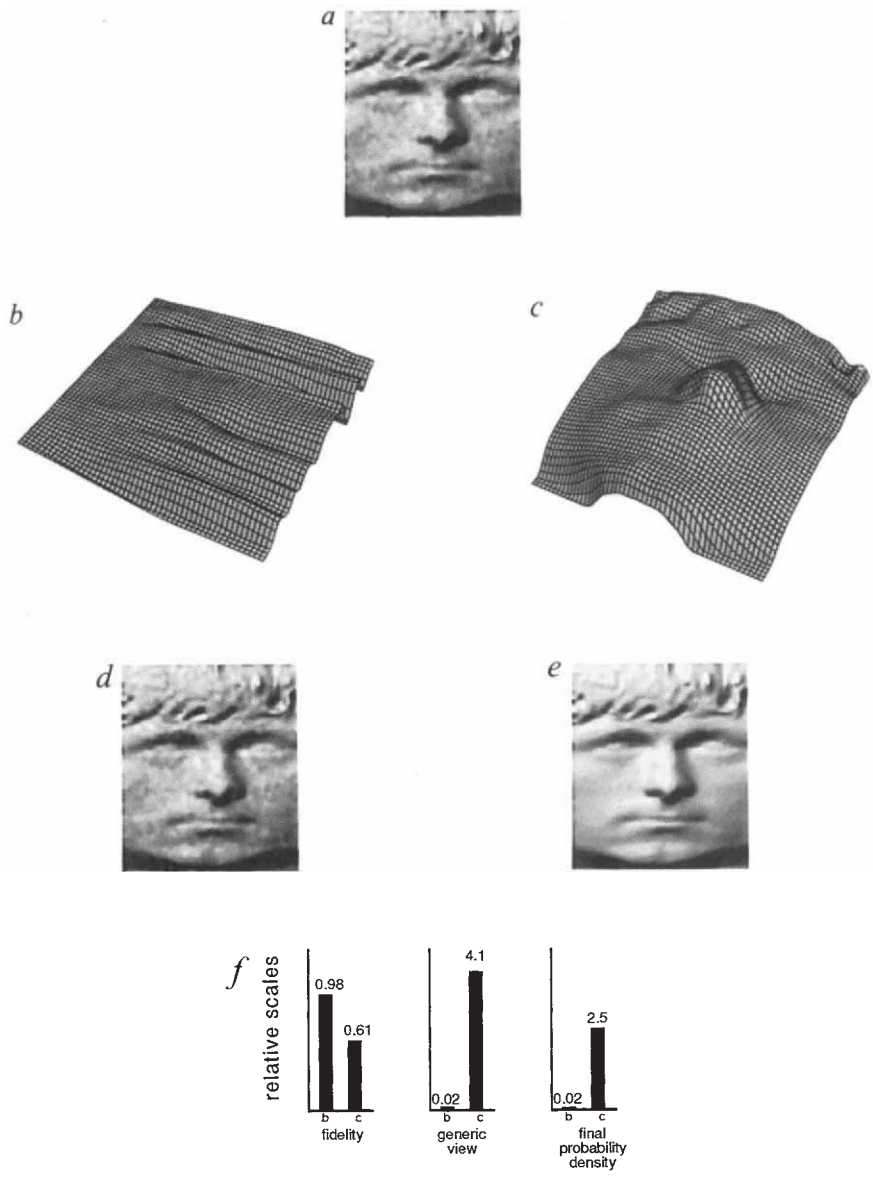

FIG. 3 Showing the need for the generic view term of equation (7). We compare the probability densities of two explanations for the image in *a*. The surface in *b* (shown at 7 × vertical exaggeration), lit at a grazing angle, yields the image in *d*. The surface in *c* gives the image in *e*, which accounts less well for the image in *a*. Thus, based on an image fidelity criterion, *b* is a better explanation. The common prior assumption of a smooth surface[14] would also favour *b* (the surface is very smooth at the true vertical scale). However, the object and light source must be precisely positioned for the shape in *b* to give the image in *d*; the generic view term of the scene probability equation (7) penalizes this. Including the generic view term makes the overall probability densities (shown in *f*), favour the perceptually reasonable explanation of shape *c* over shape *b*. (We made this example by construction. Gaussian random noise at a 7 dB signal-to-noise ratio was added to *e* to make *a*; *b* was found from *a* using a shape from shading algorithm, assuming constant surface height at the left picture edge[23]. We evaluated the likelihood of *b* and *c*, assuming both generic object pose and generic lighting direction[24]. The strength of a prior preference for smooth surfaces is arbitrary and none was included in the final densities. The actual noise variance was used for σ^2 in the fidelity term of equation (7), although a wide range of assumed variances would give the preferences shown here.)

scene parameters $\vec{\beta}$ given the visual data $\vec{y}$:

$$P(\vec{\beta}\,|\,\vec{y}) = k \exp\left(\frac{-\|\vec{y}-\vec{f}(\vec{x}_0,\vec{\beta})\|^2}{2\sigma^2}\right) P_{\vec{\beta}}(\vec{\beta})\,\frac{1}{\sqrt{\det(\mathbf{C})}} \qquad (7)$$

$$= k\ \text{(fidelity) (prior probability) (generic view)}$$

where the i and jth elements of the matrix $\mathbf{C}$ are

$$C_{ij} = \vec{f}'_i \cdot \vec{f}'_j - (\vec{y}-\vec{f}(\vec{x}_0,\vec{\beta})) \cdot \vec{f}''_{ij} \qquad (8)$$

We call equation (7) the scene probability equation. The normalization constant k does not enter into comparisons between interpretations $\vec{\beta}$. The exponential term, which we call the image fidelity term, favours scene hypotheses that have a small mean-squared difference from the visual data. This and the prior probability term $P_{\vec{\beta}}(\vec{\beta})$ are familiar in computational vision. Regularization, from which many vision algorithms have been derived[12,13], finds the maximum probability density[14,15] using these two terms, when viewed in a bayesian context. The third, generic view term, accounts for the assumptions of generic viewpoint, pose or lighting position. The scene probability equation favours interpretations that can generate the observed image over a relatively large range of generic variables, by penalizing large image derivatives with respect to those variables. If the prior probability of the generic variable were not constant, then the factor $P_{\dot{x}}(\dot{x}_0)$ would be included in the prior term of equation (7).

The generic view term is especially useful when several explanations account equally well for visual data, as occurs commonly in problems of stereo, shape, motion and colour perception; ref. 16, for example. Then the image fidelity term is the same for the competing explanations. The prior probabilities may not be known well[4]. The generic view term allows a choice based on the relatively reliable assumptions of generic view, pose, or light source position.

Our approach relates to bayesian analyses of data interpolation, image restoration and other problems[11,15,17]. In that work, as in this, one favours hypotheses that could have generated the observed data in many ways (see also ref. 18, a related non-bayesian approach).

Using the scene probability equation (7), we plot in Fig. 1*e* the relative probabilities of shapes 1–5 of Fig. 1*b*. Note the agreement with the bump/dimple shapes perceived to be the true explanation of Fig. 1*a*. (Presumably, these are perceptually favoured because they are more probable.) Without the generic

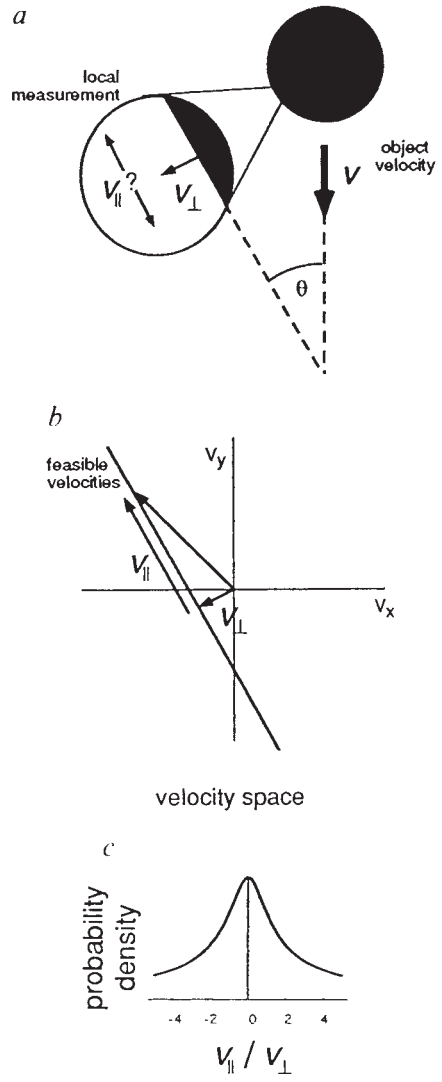

FIG. 4 Application of the scene probability equation to velocity estimation. *a*, Within a local aperture, the object velocity direction is ambiguous[19]. $V_\perp$, the component of velocity normal to the local contrast, is constrained by the measurement, while $V_\parallel$ is unconstrained. *b*, Line in velocity space of object velocities consistent with observed normal velocity. High values of $V_\parallel$ imply a concidental alignment of the local contrast orientation with the object velocity direction. In our framework, the measurement vector $\bar{y}$ is the normal velocity vector; the scene parameter $\bar{\beta}$ is $V_\parallel$; the generic variable $\bar{x}$ is the angle θ between the object velocity and the orientation of local contrast. The scene probability equation (7), penalizes high derivatives of the normal velocity with respect to contrast orientation. *c*, Resulting posterior probability for $V_\parallel$, showing a bias in favour of the normal velocity ($V_\parallel = 0$). This bias is consistent with psychophysical observations[20].

view term, one would have to state an arbitrary preference for bumps or dimples to choose between the candidate shapes.

In Fig. 2 we use the scene probability equation to choose between surface reflectance functions in a case where they would otherwise be indistinguishable. Figure 3 shows an example in which both the fidelity and the prior probability terms favour a perceptually implausible explanation. Only when the generic view term of equation (7) is included does the perceptually favoured explanation rank higher.

In Fig. 4, we apply the scene probability equation to the problem of estimating the local image velocity from local measurements of the velocity components normal to the contrast orientation[19]. All velocity components parallel to the local contrast orientation are possible, but high speeds would imply a coincidental alignment of the local contrast with the image velocity. The scene probability equation predicts a bias toward zero parallel velocity component, which is supported by psychophysical evidence[20].

From an equation that ranks scene interpretations, such as the scene probability equation (equation (7)), one can develop vision algorithms that find an optimum interpretation. Including the generic view term gives a better statistical model of the visual world. It may result in more powerful and accurate algorithms for vision. □

Received 13 September 1993; accepted 27 January 1994.

1. Koenderink, J. J. & van Doorn, A. J. *Biol. Cybern.* **32,** 211–216 (1979).
2. Binford, T. O. *Art. Intel.* **17,** 205–244 (1981).
3. Biederman, I. *Comp. Vis. Graph. Image Proc.* **32,** 29–73 (1985).
4. Nakayama, K. & Shimojo, S. *Science* **257,** 1357–1363 (1992).
5. Lowe, D. G. & Binford, T. O. *IEEE Pat. Anal. Mach. Intel.* **7,** 320–326 (1985).
6. Malik, J. *Intl. J. Comp. Vis.* **1,** 73–103 (1987).
7. Richards, W. A., Koenderink, J. J. & Hoffman, D. D. *J. Opt. Soc. Am. A.* **4,** 1168–1175 (1987).
8. Pentland, A. P. *Intl. J. Comp. Vis.* **1,** 153–162 (1990).
9. Leclerc, Y. G. & Bobick, A. F. in *Proc. IEEE Computer Vision and Pattern Recognition* 552–558 (Maui, Hawaii, 1991).
10. Jepson, A. D. & Richards, W. *Spatial Vision in Humans and Robots* (eds Harris, L. & Jenkin, M.) (Cambridge Univ. Press, UK, 1992).
11. Berger, J. O. *Statistical Decision Theory and Bayesian Analysis* (Springer, New York, 1985).
12. Tikhonov, A. N. & Arsenin, V. Y. *Solutions of Ill-posed Problems* (Winston, Washington DC, 1977).
13. Poggio, T., Torre, V. & Koch, C. *Nature* **317,** 314–319 (1985).
14. Terzopoulos, D. *IEEE Pat. Anal. Mach. Intell.* **8,** 413–424 (1986).
15. Szeliski, R. *Bayesian Modeling of Uncertainty in Low-level Vision* (Kluwer Academic, Boston, 1989).
16. Marr, D. C. *Vision* (Freeman, New York, 1982).
17. MacKay, D. J. C., *Neural Comput.* **4,** 415–447 (1992).
18. Weinshall, D., Werman, M. & Tishby, N. *Proc. 3rd Eur. Conf. Computer Vision* (Springer, Stockholm, 1994).
19. Horn, B. K. P. & Schunk, B. G. *Artif. Intel.* **17,** 185–203 (1981).
20. Nakayama, K. & Silverman, G. H. *Vision Res.* 739–746 (1988).
21. Cook, R. L. & Torrance, K. E. in *SIGGRAPH-81* (Special Interest Group on Computer Graphics Conf. Proc. Assoc. for Computing Machinery, New York, 1981).
22. Freeman, W. T. in *Proc. 4th Intl. Conf. Computer Vision* 347–356 (IEEE, Berlin, Germany, 1993).
23. Bichsel, M. & Pentland, A. P. in *Proc. IEEE Computer Vision and Pattern Recognition* 459–465 (Champaign, IL, 1992).
24. Freeman, W. T. *Intl. J. Comp. Vis.* (in the press).

ACKNOWLEDGEMENTS. I thank E. Adelson, D. Brainard, D. Knill, K. Nakayama, E. Simoncelli, R. Szeliski and A. Yuille for discussion and suggestions. Much of this research was performed at the MIT Media Laboratory and was supported by a contract from David Sarnoff Research Laboratories (subcontract to the National Information Display Laboratory) to E. Adelson.

Direct modulation by Ca^{2+}–calmodulin of cyclic nucleotide-activated channel of rat olfactory receptor neurons

Tsung-Yu Chen & King-Wai Yau

Department of Neuroscience and Howard Hughes Medical Institute, The Johns Hopkins University School of Medicine, Baltimore, Maryland 21205, USA

OLFACTORY receptor neurons depolarize in response to odorant stimulation of their sensory cilia[1–3]. One transduction mechanism involves a G-protein-mediated increase in adenylate cyclase activity[4–8], raising the internal cyclic AMP concentration to open a cyclic nucleotide-activated cation channel on the plasma membrane[9–14]. An influx of Ca^{2+} through this channel, which is permeable to both monovalent and divalent cations, triggers olfactory adaptation[15]. Previous work has indicated that at least part of this Ca^{2+}-mediated adaptation resides in the channel itself[15–17], but the mechanism remains unclear and controversial[16–18]. Here we use the cloned channel from rat[19] expressed in a cell line and the native channel from rat olfactory receptor cells to show that Ca^{2+} reduces the apparent affinity of the channel for cAMP by